SCIENCE CHINA
Earth Sciences

• RESEARCH PAPER •

September 2013 Vol.56 No.9: 1510–1518
doi: 10.1007/s11430-013-4636-z

# Microstructures and deformation mechanisms of hornblende in Guandi complex, the Western Hills, Beijing

ZHANG XiaoLi[1,2,4], HU Ling[2*], JI Mo[2,3], LIU JunLai[2] & SONG HongLin[2]

[1] *Key Laboratory of Petroleum Resources Research, Institute of Geology and Geophysics, Chinese Academy of Sciences, Lanzhou 730000, China;*
[2] *State Key Laboratory of Geological Processes and Mineral Resources, China University of Geosciences, Beijing 100083, China;*
[3] *China National Off-shore Oil Corporation Research Institute, Beijing 100027, China;*
[4] *School of Resource and Earth Science, China University of Mining and Technology, Xuzhou 221116, China*

Received October 15, 2012; accepted March 28, 2013; published online July 18, 2013

Multiple methods were applied to study the deformation characteristics of hornblende in Archean plagioamphibolite mylonite from the Western Hills (Beijing), including optical microscopy (OM), electron backscatter diffraction (EBSD), transmission electron microscopy (TEM), and electron probe microanalysis (EPMA). The hornblendes are $\sigma$ and $\delta$ type porphyroclasts with the new-born needle shaped grains as their tails. The analysis of lattice preferred orientation (LPO) of both the porphyroclasts and the new-born grains shows that the main slip system of the deformed hornblende is (100)<001>, suggesting that the fabric characteristics of new-born grains inherit that of porphyroclasts. Sub-microstructures show the porphyroclast core is dominated by dislocation tangle, little or no dislocations in the new-born grains, and the subgrains confined by dislocations in the transition zone between porphyroclasts and new-born grains. By using plagioclase-hornblende geothermometry and hornblende geobarometry, the estimated temperature and pressure of porphyroclasts are 675.3–702.9°C and 0.29–0.41 GPa and those of new-born grains are 614.1–679.0°C and 0.11–0.31 GPa. The bulging recrystallization is summarized as deformation mechanisms of hornblende by the discussions of the microstructures, EBSD fabric, sub-microstructures, and the deformed temperature and pressure.

**the Western Hills (Beijing), Guandi complex, hornblende, bulging recrystallization**

**Citation:** Zhang X L, Hu L, Ji M, et al. Microstructures and deformation mechanisms of hornblende in Guandi complex, the Western Hills, Beijing. Science China: Earth Sciences, 2013, 56: 1510–1518, doi: 10.1007/s11430-013-4636-z

Hornblende, together with olivine, pyroxenes, feldspar, biotite, quartz, and calcite, are the seven most common major rock-forming minerals in the lithosphere. An improved understanding of the structures, rheological characteristics, and dynamic evolution of the crust and mantle is established on the study of these major rock-forming minerals [1–3]. However, owing to the lack of feasible approaches and techniques, the contribution of hornblende to the mechanical and rheological characteristics of the lower crust is still poorly known [4, 5]. Previous researches indicate that the slip systems of hornblende are (100)[001], (010)[001], and (100)[010] [6–8], and slip occurs preferentially on (100)[001] because no TOT-type structure is broken on this plane [9]. Under experimental conditions, hornblende can widely develop $(\bar{1}01)$ deformation twins, with rare (100) twins [10]. However, in natural conditions, hornblende commonly develops (100) mechanical twins [11–13]. Hornblende occurs in rocks of various tectonic settings, and can record the dynamic processes of different structural levels. At lower temperature and/or with fluids participation, cataclastic flow and dissolution creep (diffusion creep) [8, 14] are the main deformation mechanisms of hornblende. The

*Corresponding author (email: hulin1028@gmail.com)

fine-grained matrix in the core-mantle structure is probably formed by cataclastic flow rather than dynamic recrystallization because of the brittle deformation of hornblende caused by its perfect cleavage paralleling to {110}. In low temperature and/or high strain conditions, the deformation of hornblende is fulfilled by ($\bar{1}$01) or (100) twining and (100) [001] slipping. At the same time, because the chemical components change plays a more important part than that of strain, hornblende is often decomposed into amphiboles with different components [15, 16] or other minerals, such as epidote, albite and biotite etc. [17]. Under high temperature above 650–700°C and /or low strain conditions, hornblende in dry rocks with lower aquifer fluid will show crystal plastic deformation, namely, deforming by subgrain rotation recrystallization and recovery, and slip on (hk0)[001], {110}1/2 〈1$\bar{1}$0〉 and (100)[100]. Subgrains grow paralleling to *c*-axis with boundaries composed of [001], [100] or <110> dislocations, which parallel to {110}, {100} or {010} [18, 19], respectively. Passchier et al. [8] think that it is difficult for hornblendes to deform by crystal plasticity, and their ductile deformation temperature is even higher than that of olivine. In summary, due to the lack of suitable research means and technical methods, hornblende, as a kind of biaxial hydrous minerals, is still not well known now about its deformation behaviors and mechanisms, especially the deformation mechanism of dynamic recrystallization under conditions of brittle-ductile transition.

The deformation of hornblende in Archean plagioamphibolite mylonite from the Western Hills (Beijing) has been systematically analyzed by optical microscope (OM), electron backscatter diffraction (EBSD), transmission electron microscope (TEM), and electron probe microanalysis (EPMA). The typical brittle-ductile transition characteristics in the epidote-amphibolite facies were observed and the bulging recrystallization is summarized as deformation mechanism of hornblende. The estimated temperature and pressure of hornblende developing bulging recrystallization are 614.1–679.0°C and 0.11–0.31 GPa. This research provides a basis for further studying the recrystallization mechanisms of hornblende in brittle-ductile transition conditions.

## 1 Regional geological setting

The Western Hills, in southwestern Beijing, are located in the junction of the NNE trending Taihang Mountains and the E-W trending Yanshan orogenic belt (Figure 1). Outcropped strata in the study area include Archean, Meso- to Neo-proterozoic, Paleozoic, Mesozoic, and Cenozoic. Guandi complex is exposed in the southern and northern sides of Fangshan pluton as stripes with a total area of 0.37 km$^2$. SHRIMP U-Pb zircon analysis indicates that Guandi complex has an age of 2500 Ma [20–22]. The main lithology includes biotitic amphibole plagioclase gneiss, plagioamphibolite mylonite and biotite amphibolite granulite etc., belonging to basement gneiss series.

The Guandi complex experienced multiple deformations [22, 23]. SHRIMP U-Pb zircon analysis of diorite vein in Nanjiao area determined by Wang et al. [22] indicates that this diorite vein has an age of 136±1 Ma, and the $^{40}$Ar/$^{39}$Ar age of muscovite and sericite minerals within stretching lineation ranges from 133±1 to 127±1 Ma. The diorite veins, deformed muscovite and sericite have the same age, suggesting that the study area experienced detachment and synkinematic magmatisms. Yan et al. [23] proposed that an extensional deformation happened here in the Middle to Late Triassic. The time span and mechanisms of detachment are still in dispute [22–24]. However, it is no doubt that the detachment provides the background and stress for the deformation of hornblende. In this paper, the plagioamphibolite mylonite samples were collected from Dongling area, northern margin of the Fangshan pluton. The lineation structure, composed by elongate hornblende grains, can be observed clearly in samples, providing a good opportunity to study the dynamic recrystallization mechanisms of deformed hornblende.

## 2 Analytical methods

The orientated thin sections were cut paralleling to lineation and vertical to foliation. The observation was done in the Geological Laboratory Center, China University of Geosciences (Beijing). The EBSD fabric of hornblende porphyroclasts systems were measured in the Rock Fabric Laboratory. *XZ* sections (paralleling to lineation and normal to foliation) were cut from the samples and polished using BUEHLER MASTERMET colloidal silica and BUEHLER grinder-polisher. The LPO data acquisition was done on a Hitachi S-3400N-II scanning electron microscope mounted with Nordlys EBSD Model NL-II detector. The thin sections surface was inclined 70° to the incidental beam. The new technique provides a fast data acquisition for mineral grains or a portion thereof with 0.1 μm spatial resolution and 0.5° angular resolution. A 15 kV acceleration voltage was applied and the working distance was 23 mm. EBSP analysis was completed using the HKL Channel 5 software package. The sub-microstructures of hornblende porphyroclasts systems were observed in the Transmission Electron Laboratory, with the instrument of high-resolution transmission electron microscopy of type Hitachi H-8100. The chemical components of hornblende and plagioclase were identified by EDAX9100 spectrum during transmission electron microscope (TEM) analysis, with the operating voltage of 10 kV, the current of 5mA, the power of 50 VA, the beam of 200 μA and the beam diameter of 1–2.5 μm. The mineral components were quantitatively analyzed in the Electron Probe Laboratory, with the instrument of EPMA-1600 electron microprobe.

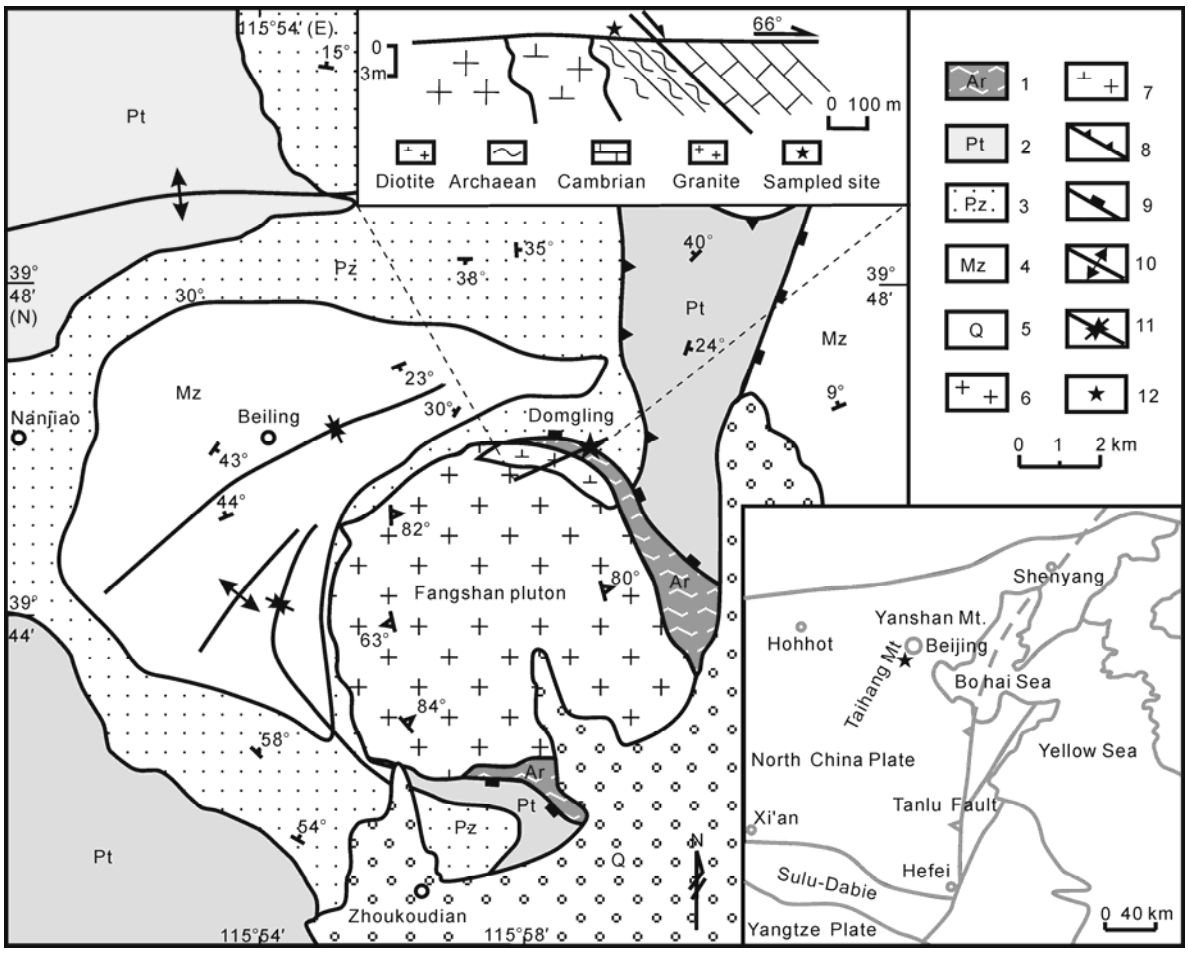


**Figure 1** Geological setting sketch of the Western Hill (Beijing) [24]. 1, Archaean; 2, Proterozoic; 3, Paleozoic; 4, Mesozoic; 5, Quaternary; 6, granite; 7, diorite; 8, reverse fault; 9, normal fault; 10, anticline lines; 11, syncline lines; 12, sampled site.

## 3 Deformation microstructures

The studied plagioamphibolite mylonite samples are composed of hornblende of more than 50%, plagioclase of about 30%, and quartz of 10%.

Core-mantle structure (Figure 2(a)) and porphyroclast fabric were observed in amphibolite mylonite. The hornblendes are $\sigma$ and $\delta$ type porphyroclasts (Figure 2(b), (c)) of 0.1–0.5 mm in size, in which cleavage microcrack and undulatory extinction were observed. The strongly curved boundaries of hornblende porphyroclasts bulge towards tails, suggesting that bulging recrystallization may be the main dynamic recrystallization mechanism. Tails of porphyroclasts systems were composed of new-born needle shaped hornblende grains. These tiny grains (0.03–0.08 mm in length) were obviously elongated, the long axis of which parallel to or intersect in low angle with the stretching lineation. The rigid porphyroclasts of subhedral hornblende (Figure 2(d)) also can be seen in thin sections, as the result of the different azimuth between the crystalline orientation of hornblende and regional shearing[1)].

The plagioclase deformed into core-mantle structure, or even into banded structure as the subgrain rotation recrystallization. The myrmekite in the K-feldspar porphyroclasts can be observed.

## 4 EBSD LPO characteristics

LPO measurements were performed on hornblende grains using interactive mode. Several representative windows (8 – 9) are chosen for LPO data acquisition. Most of these windows contained representative hornblende grains. Data from all the windows were merged to form the sample data

1) Liu J L, Cao S Y, Song Z J, et al. Mineral lattice preferred orientation and brittle-ductile deformation in mylonitic rocks (in Chinese). In: National Tectonic and Structure 4th Conference, 2008. October 10–13, Beijing.

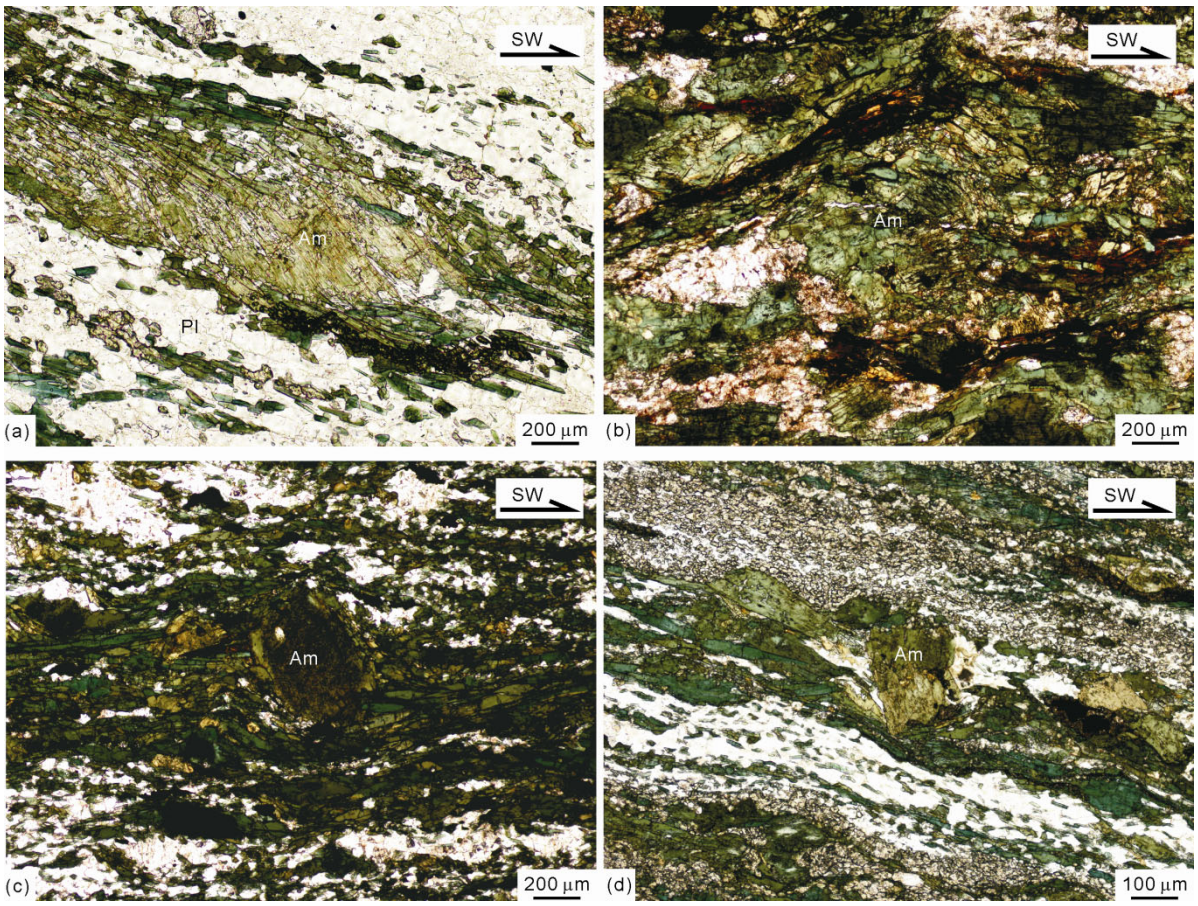


**Figure 2** Microstructures of deformed hornblende. (a) Core-mantle structure of hornblende; (b) $\sigma$ type porphyroclast and new-born needle shaped grains of hornblende; (c) $\delta$ type porphyroclast and new-born needle shaped grains of hornblende; (d) rigid porphyroclasts of subhedral hornblende.

set. The interactive mode is a reliable way of collecting EBSP data from representative grains or subgrains in the field of view. All the LPO data are presented with an equal area, lower hemisphere projection in a structural frame of foliation paralleling to the *XY* plane and lineation paralleling to the *X* direction (Figure 3). The LPO of porphyroclasts shows that <100> parallels to *Z*, <001> parallels to *X*, and <010> parallels to the *Y* axis, reflecting a slip system of (100) <001>. The LPO of tails shows that <100> parallels to *Z*, <001> parallels to *X*, and <010> parallels to the *Y* axis, reflecting a main slip system of (100) <001>. As the same LPO, it suggested an inheritance from the porphyroclasts to tails.

## 5 Sub-microstructures

Different dislocation combinations occurred regularly from porphyroclasts (sample DL-8-3) to tails (sample DL-8-6). In hornblende porphyroclasts, there are dislocation tangles (Figure 4(a)) primarily, and also dislocation arrays (Figure 4(b)) and elongated straight free dislocations (Figure 4(c)) regionally. Free dislocations, dislocation arrays, subgrains and twins can be found in the transition zone between porphyroclasts and tails. As well organized free dislocations, the presentation of dislocation arrays (Figure 4(d)) and dislocation walls indicated the decrease of free energy, which is an essential procedure of hornblende's dynamic recrystallization. The subgrain is defined as portion of a crystal or grain with an orientation that differs slightly from the orientation of neighboring portions of the same crystal. The occurrence of subgrains (Figure 4(e)) in the transition zone between porphyroclasts and tails indicated the deformation by dislocation climb and recovery. Few hornblende twins (Figure 4(f)), with the dislocation of nearly 90° offset, were observed by TEM. It is considered that the presentation of very few hornblende twins cannot contribute to dynamic recrystallization of hornblende in this study. It is different from the research of twinning nucleation recrystallization of amphibolite rocks in Diancangshan area [13]. Consistent with the law that free energy decreased from old to new grains during dynamic recrystallization, different dislocation combinations occurred regularly and the free energy decreased from porphyroclasts to tails.

In tails, the straight boundaries can be found in new-born grains whose long axis nearly parallels to [001]. These new-born grains have no (Figure 4(g)) or little dislocations (Figure 4(h)), with the dislocation density of $5.0 \times 10^8/\text{cm}^2$.

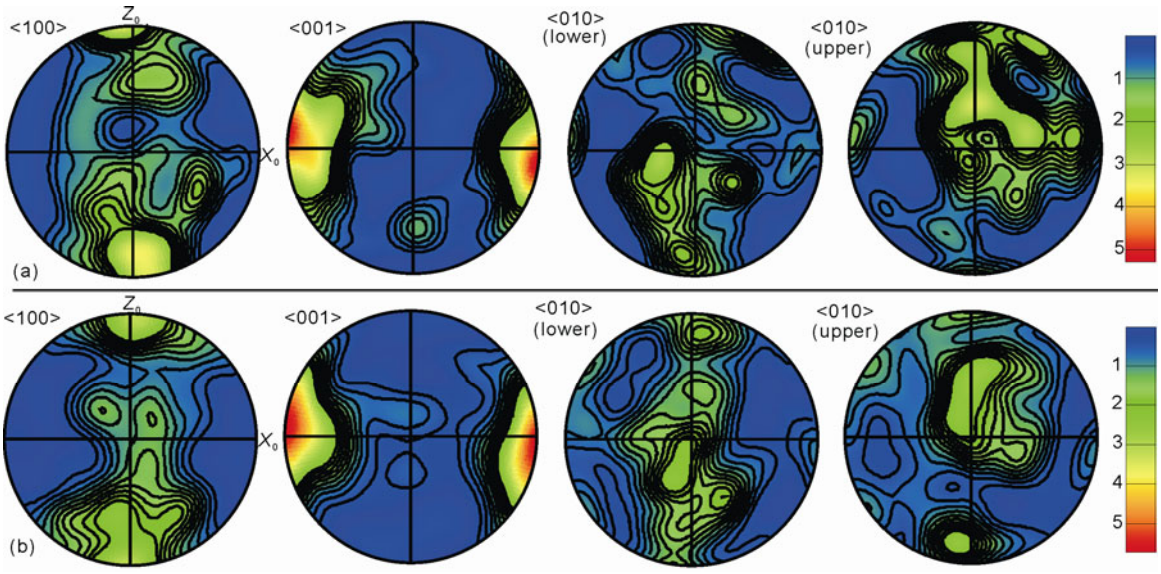


**Figure 3** EBSD-measured LPO of hornblende. (a) Hornblendes in porphyroclasts (equal area, lower hemisphere projection, 264 data points ); (b) hornblendes in tails (equal area, lower hemisphere projection, 257 data points).

The dislocations (Figure 4(i)) that parallel to [001] within particles might be developed during the dynamic recrystallization.

## 6 Mineral chemistry and deformation *P-T* conditions

The chemical components of hornblende and plagioclase were obtained by Electronic Probe Technique as shown in Table 1. The hornblendes were classified according to IMA78 by Leake [25], in which the maximum of $Fe^{3+}$ was calculated using the 13eCNK method of Lin et al. [26]. It is classified into magnesio-hornblende primarily (Figure 5(a)). The bivariate diagram (Figure 5(b)) of $Al^{IV}$– $Al^{VI}$ shows that hornblende of porphyroclasts deformed in amphibolite faces and hornblende of tails developed in epidote amphibolite faces.

The hornblende-plagioclase geothermometry [27] and various hornblende geobarometry [28–32] were used to estimate the deformation temperature and pressure in this study. Anderson et al. [32] emphasized on estimation of temperature and oxygen fugacity preferentially. Besides appropriate buffered mineral assemblages, the $Fe^{3+}/(Fe^{2+}+Fe^{3+})$ value should be higher than 0.25 or 0.20 (suggested by Schmidt [31]) and the $Fe^{tot}/(Fe^{tot}+Mg)$ value should range from 0.40 to 0.65. Considering temperature and oxygen fugacity, we finally selected the geobarometer method by Anderson et al. [32].

Table 1 and Figure 5(c) show the deformation temperature and pressure. For the porphyroclasts series, temperature and pressure ranged from 675.3 to 702.9°C with an average of 691.2°C, and from 0.29 to 0.41 GPa with an average of 0.34 GPa, respectively. For the new-born grains in tails, the temperature and pressure ranged from 614.1 to 679.0°C with an average of 636.6°C, and from 0.11 to 0.31 GPa with an average of 0.20 GPa, respectively. The new-born hornblendes in tails were developed by ductile shearing from porphyroclasts. Therefore, the estimated temperature and pressure of new-born hornblendes in tails represent the deformation condition that is from 614.1 to 679.0°C and from 0.11 to 0.31 GPa, respectively.

## 7 Discussions

### 7.1 Dynamic recrystallization mechanisms of hornblende

The dynamic recrystallization includes bulging, subgrain rotation, and high-temperature grain boundary migration recrystallization, developed with the increasing of temperature. An improved understanding of the structures, rheological characteristics, and dynamic evolution of the crust and upper mantle is established on the dynamic recrystallization studies of quartz [8], calcite [33], and feldspar [34]. Hornblende occurs in the rocks of various tectonic settings, and can record the dynamic processes of different structural levels from shal-low to deep crust. Therefore, it is necessary to study deformation mechanisms of hornblende.

The development of porphyroclasts fabric and obviously fine-grained new-born hornblende grains, observed in amphibolite mylonite from the Western Hills, Beijing, indicates the dynamic recrystallization of brittle-ductile transitional deformation. The strongly curved boundaries of hornblende porphyroclasts bulge towards tails. Consistent with the law that free energy decreased from old to new grains during dynamic recrystallization, different disloca-

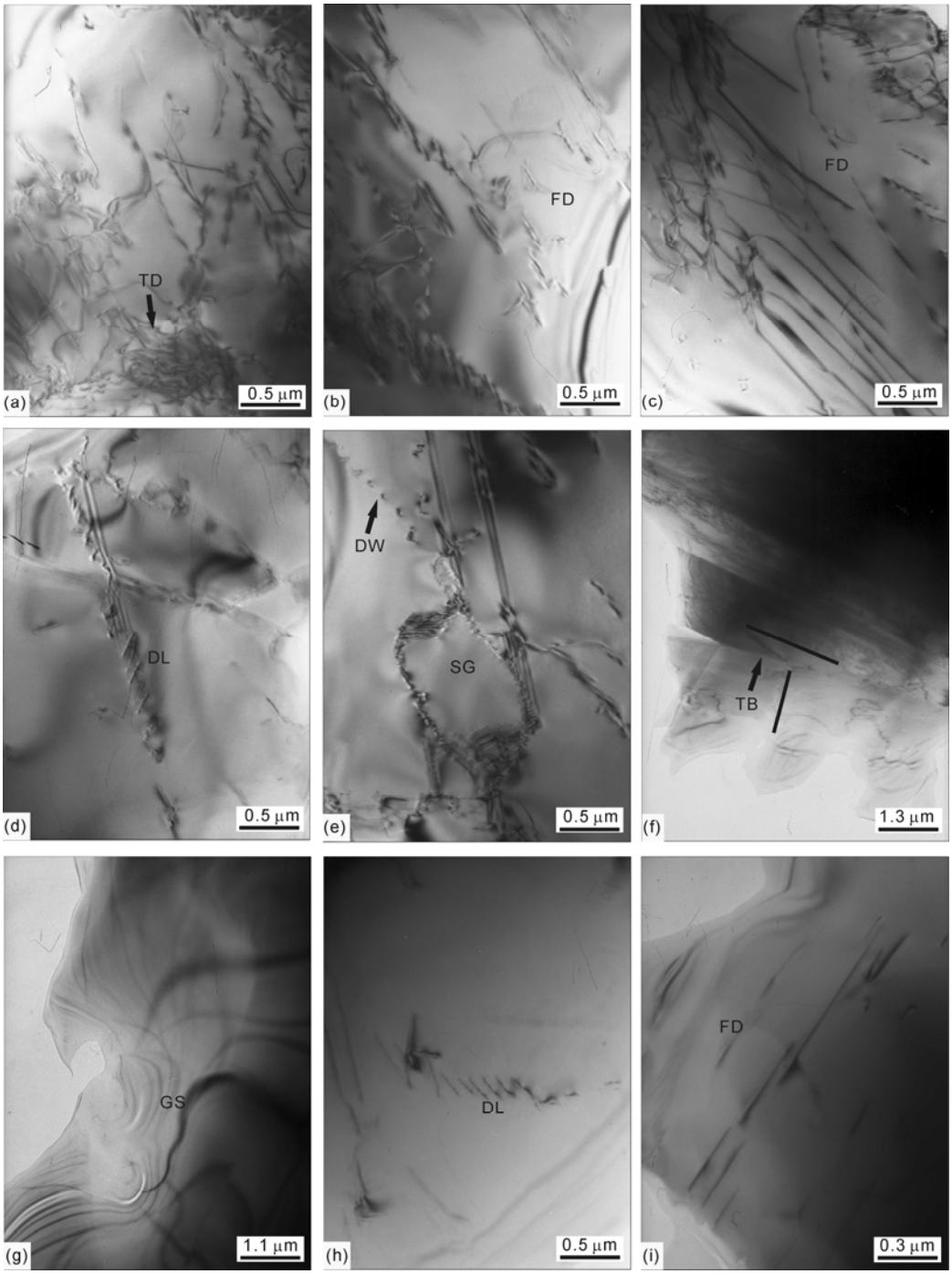


**Figure 4** TEM sub-microstructural characteristics of hornblende. (a)–(c) Sub-microstructures of hornblendes porphyroclasts: (a) dislocation tangle, DL-8-3; (b) untypical dislocation array, DL-8-3; (c) elongated straight free dislocation, DL-8-3. (d)–(f) Sub-microstructures of hornblendes in the transition zone between porphyroclasts and tails: (d) dislocation array, DL-8-3; (e) subgrain, DL-8-3; (f) Hornblende twins, DL-8-3. (g)–(i) Sub-microstructures of new-born hornblende grains in tails: (g) gratings stripes and no dislocations, DL-8-6; (h) dislocation array, DL-8-6; (i) free dislocation parallel to [001], DL-8-6. FD-Free dislocation; DA-dislocation array; DT-dislocation tangle; TB-twin boundary; GS-gratings stripes.

tion combinations occurred regularly and the free energy decreased from porphyroclasts to tails. The analysis of LPO of both the porphyroclasts and the new-born grains shows that the main slip system of the deformed hornblende is (100)<001>, suggesting that the fabric characteristics of new grains inherit those of porphyroclasts. The estimated temperature and pressure of hornblende developing bulging recrystallization are 614.1–679.0°C and 0.11–0.31 GPa, reflecting the rheological deformation condition of the middle crust.

The typical brittle-ductile transition characteristics in the epidote-amphibolite facies were observed and the bulging

**Table 1** Results of temperature and pressure estimations[a)]

| Sample | Porphyroclasts | | | | Tails | | | | |
|---|---|---|---|---|---|---|---|---|---|
| | DL-8-3 | DL-8-5 | DL-8-9 | DL-8-4 | DL-8-1 | DL-8-2 | DL-8-6 | DL-8-7 | DL-8-8 |
| Chemical components of hornblendes | | | | | | | | | |
| $SiO_2$ (wt%) | 46.7 | 47.5 | 47.3 | 46.3 | 50.9 | 50.7 | 49.3 | 48.3 | 51.7 |
| $TiO_2$ (wt%) | 0.7 | 0.6 | 0.8 | 0.6 | 0.3 | 0.6 | 0.1 | 0.5 | 0.4 |
| $Al_2O_3$ (wt%) | 8.0 | 7.5 | 7.6 | 8.5 | 5.1 | 5.8 | 7.2 | 6.8 | 5.0 |
| FeO (wt%) | 14.4 | 14.0 | 14.4 | 14.2 | 12.5 | 11.5 | 13.3 | 13.1 | 12.2 |
| MgO (wt%) | 13.5 | 14.4 | 14.3 | 13.2 | 15.5 | 16.2 | 14.5 | 14.7 | 16.2 |
| MnO (wt%) | 0.5 | 0.3 | - | 0.2 | 0.3 | 0.3 | 0.1 | 0.6 | 0.4 |
| CaO (wt%) | 11.1 | 10.6 | 10.9 | 11.8 | 11.5 | 11.3 | 11.0 | 11.3 | 11.2 |
| $Na_2O$ (wt%) | 1.7 | 1.7 | 1.4 | 1.9 | 1.0 | 1.0 | 1.3 | 1.2 | 1.1 |
| $K_2O$ (wt%) | 0.59 | 0.6 | 0.65 | 0.59 | 0.24 | 0.38 | 0.45 | 0.4 | 0.01 |
| Total (wt%) | 97.19 | 97.20 | 97.35 | 97.29 | 97.34 | 97.78 | 97.25 | 96.90 | 98.21 |
| $Al^{iv}$ (wt%) | 1.07 | 0.99 | 1.03 | 1.14 | 0.60 | 0.70 | 0.80 | 0.89 | 0.60 |
| $Al^{vi}$ (wt%) | 0.32 | 0.31 | 0.30 | 0.35 | 0.27 | 0.28 | 0.43 | 0.29 | 0.25 |
| Chemical components of plagioclases | | | | | | | | | |
| $SiO_2$ (wt%) | 60.56 | 60.04 | 60.92 | 60.15 | 61.07 | 61.73 | 62.13 | 60.07 | 59.91 |
| $TiO_2$ (wt%) | - | 0.33 | - | - | - | - | - | 0.01 | 0.13 |
| $Al_2O_3$ (wt%) | 23.96 | 23.62 | 23.38 | 24.59 | 23.95 | 23.4 | 22.87 | 23.81 | 23.46 |
| FeO (wt%) | 0.42 | 0.29 | 0.23 | 0.17 | 0.02 | 0.15 | 0.19 | 0.42 | 0.16 |
| MgO (wt%) | - | - | - | 0.21 | - | 0.02 | 0.08 | 0.09 | - |
| MnO (wt%) | - | 0.06 | - | - | - | - | - | 0.01 | 0.22 |
| CaO (wt%) | 4.96 | 5.01 | 5.09 | 5.36 | 4.85 | 5.01 | 4.66 | 5.71 | 5.08 |
| $Na_2O$ (wt%) | 10.05 | 9.91 | 10.29 | 9.95 | 9.83 | 10.54 | 10.21 | 9.83 | 9.99 |
| $K_2O$ (wt%) | 0.11 | - | 0.04 | - | 0.17 | 0.03 | 0.04 | 0.14 | - |
| Total (wt%) | 100.06 | 99.26 | 99.95 | 100.43 | 99.89 | 100.88 | 100.18 | 100.09 | 98.95 |
| Ab (%) | 0.78 | 0.75 | 0.72 | 0.80 | 0.78 | 0.77 | 0.78 | 0.78 | 0.78 |
| An (%) | 0.22 | 0.24 | 0.25 | 0.20 | 0.21 | 0.23 | 0.22 | 0.21 | 0.22 |
| temperature and pressure estimations | | | | | | | | | |
| $T$ (°C) | 694.0 | 702.9 | 692.5 | 675.3 | 620.3 | 626.7 | 614.1 | 679.0 | 642.9 |
| $P1$ (GPa) | 0.31 | 0.26 | 0.28 | 0.36 | 0.05 | 0.10 | 0.23 | 0.20 | 0.04 |
| $P2$ (GPa) | 0.31 | 0.26 | 0.27 | 0.36 | 0.02 | 0.08 | 0.22 | 0.19 | - |
| $P3$ (GPa) | 0.24 | 0.20 | 0.22 | 0.28 | 0.02 | 0.07 | 0.17 | 0.15 | 0.01 |
| $P4$ (GPa) | 0.36 | 0.32 | 0.33 | 0.41 | 0.11 | 0.17 | 0.28 | 0.26 | 0.10 |
| $P5$ (GPa) | 0.34 | 0.29 | 0.32 | 0.41 | 0.12 | 0.18 | 0.31 | 0.26 | 0.11 |
| Average | 691.2°C, 0.34 GPa | | | | 636.6°C, 0.20 GPa | | | | |

a) The mineral components were quantitatively analyzed in the Electron Probe Laboratory, China University of Geosciences (Beijing). No.19990075 EPMA-1600 electron microprobe was used. $T$ was according to Holland et al. [27]; $P1$ was according to Hammarstrom et al. [28]; $P2$ was according to Hollister et al. [29]; $P3$ was according to Johnson et al. [30]; $P4$ was according to Schmidt [31]; $P5$ was according to Anderson et al. [32].

recrystallization is summarized as deformation mechanisms of hornblende by the discussion of the microstructures, EBSD fabric, sub-microstructures, and the deformed temperature and pressure.

### 7.2 Comparisons with previous studies

In this paper, it is suggested that the deformation environment is epidote-amphibolite facies and the bulging recrystallization is the deformation mechanism of hornblende from Guandi complex in the Western Hills, Beijing. The temperature and pressure of hornblende deformation are 614.1–679.0°C with an average of 636.6°C and 0.11–0.31 GPa with an average of 0.20 GPa. It is similar to 637°C reported by Cao et al. [13] and 0.33 GPa by Yao et al. [35], reflecting the rheological deformation condition of the middle crust. It is different from the conclusion by Passchier et al. [8] that the crystal plastic deformation of hornblende is difficult and its ductile deformation temperature is even higher than that of olivine. But, it is in agreement with the conclusion by Ji et al. [36] that the brittle-ductile transitional deformation of hornblende developed between feldspar and olivine. Furthermore, our conclusion is also different from the twining nucleation recrystallizaion of hornblende under brittle-ductile transitional conditions suggested by Cao et al. [13]. On the other hand, Hu et al. [9] reported the twining nucleation recrystallizaion of hornblende is a special form of bulging recrystallization. Thus, the bulging

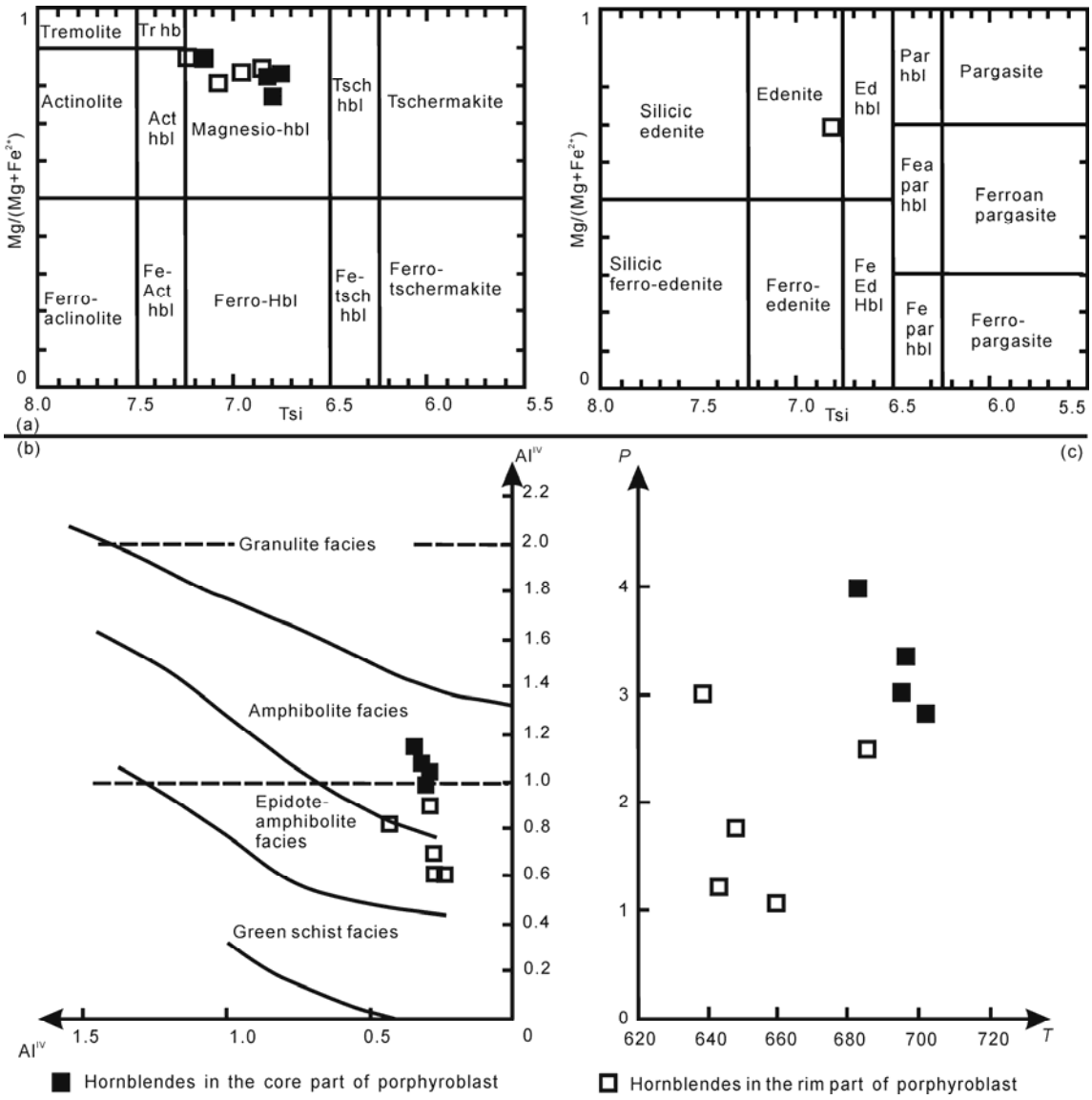


**Figure 5** Mineral chemistry of hornblende. (a) Classification of hornblendes; (b) bivariate diagram with $Al^{IV}$-$Al^{VI}$of hornblende; (c) *P-T* diagram of hornblende.

recrystalliztion in this study has a more universal meaning for brittle-ductile transitional deformation of hornblende.

## 8 Conclusions

By comprehensive analyses of the microstructures, LPO, sub-microstructures, and the deformed temperature and pressure, we can conclude:

(1) There are three major microstructures indicating the bulging recrystallization, the $\sigma$ and $\delta$ type porphyroclasts systems, the strongly curved boundaries bulging towards tails and new-born needle shaped grains. Different dislocation combinations occurred regularly from porphyroclasts to tails, consistent with the law that free energy decreased from old to new grains during dynamic recrystallization.

(2) The new-born grains and porphyroclasts have the inherited LPO, indicating a main slip system of (100)<001>. It is one of the direct proofs for bulging recrystallization.

(3) The temperature and pressure of dynamic recrystallization are estimated from 614.1 to 679.0°C and from 0.11 to 0.31 GPa, respectively, representing an epidote-amphibolite facies.

All above results, microsstructures, LPO, sub-microstructures, and deformation temperature and pressure, indicate that the deformation environment is epidote-amphibolite facies and the bulging recrystallization is the deformation mechanism of hornblende from Guandi complex in the Western Hills, Beijing.

*We are grateful to Li Shun, Cao Wentao, and Du Bingying for their help in field work, Han Yong for her help in TEM observation, Profs. Zhou Yongsheng and Lin Wei for their comments on P-T estimation, and Profs.*

*Wang Yu and Duan Yi for their constructive suggestions. This research was supported by the National Natural Science Foundation of China (Grant No. 40772133).*


1 Reymer A, Schubert G. Phanerozoic addition rates to the continental crust and crustal Growth. Tectonics, 1984, 3: 63–77
2 Kirby S H, Kronenberg A K. Deformation of clinopyroxenite: Evidence for transition in flow mechanisms and semibrittle behaviour. J Geophys Res, 1984, 89: 3177–3192
3 Liu J L, Walter J M, Weber K. Fluid-enhanced low-temperature plasticity of calcite marble: Microstructures and mechanisms. Geology, 2002, 30: 787–790
4 Brodie K H, Rutter E. On the relationship between deformation and metamorphism with special reference to the behavior of basic rocks. In: Thompson A B, Rubie D C, eds. Metamorphic Reactions: Kinetics, Textures, and Deformation. Berlin: Springer, 1985. 138–179
5 Barruol G, Kern H. Seismic anisotropy and shear-wave splitting in lower-crustal and upper-mental rocks from the Ivrea Zone-experimental and calculated data. Phys Earth Planetary Inter, 1996, 95: 175–194
6 Rooney T P, Riecker R E, Gavasci A T. Hornblende deformation features. Geology, 1975, 3: 364–366
7 Jiang Z, Skrotzki W. Microstructure and texture of hornblende from an amphibolite of the KTB main borehole (NE-Bavaria). Z Geol Wiss, 1996, 24: 657–669
8 Passchier W C, Trouw R A J. Microtectonics. Berlin: Springer, 2005. 367
9 Hu L, Liu J L, Ji M, et al. Recognition of Microtectonics (in Chinese). Beijing: Geological Publishing House, 2009. 1–83
10 Dollinger G, Blacic J D. Deformation mechanisms experimentally and naturally deformed amphiboles. Earth Planet Sci Lett, 1975, 26: 409–416
11 Biermann C. (100) Deformation twins in naturally deformed amphiboles. Nature, 1981, 292: 821–823
12 Hacker B, Christie J M. Brittle/ductile and plastic/catalastic transitions in experimentally deformed and metamaphosed amphibolite. In: Duba A G, Durham W B, Handie J W, et al, eds. Brittle-Ductile Transitions in Rocks. AGU Geophys Monogr Ser, 1990, 56: 127–148
13 Cao S Y, Liu J L, Hu L, et al. Micro- and submicrostructural evidence for high temperature brittle-ductile transition deformation of hornblende: Case study of high-grade mylonites from Diancangshan, western Yunnan. Sci China Ser D-Earth Sci, 2007, 37: 54–57
14 Aspiroz M D, Lloyd G E, Fernández C. Development of lattice preferred orientation inclinoamphiboles deformed under low-pressure metamorphic conditions: A SEM/EBSD study of metabasites from the Aracena metamorphic belt (SW Spain). J Struct Geol, 2007, 29: 629–645
15 Imon R, Okudaira T, Fujimoto A. Dissolution and precipitation processes in deformed amphibolites: An example from the ductile shear zone of the Ryoke metamorphic belt, SW Japan. J Metamorph Geo, 2002, 20: 297–308
16 Imon R, Okudairaa T, Kanagawab K. Development of shape and lattice-preferred orientations of amphibole grains during initial cataclastic deformation and subsequent deformation by dissolution-precipitation creep in amphibolites from the Ryoke metamorphic belt, SW Japan. J Struct Geol, 2004, 26: 793–805
17 Berger A, Stünitz H. Deformation mechanisms and reaction of hornblende: Examples from the *Bergell tonalite* (Central Alps). Tectonophysics, 1996, 257: 149–174
18 Skrötzki W. Defect structures and deformation mechanisms in naturally deformed hornblende. Phys Status Solid, 1992, 131: 605–624
19 Kruse R, Stüenitz H. Deformation mechanisms and phase distribution in mafic high-temperature mylonites from the Jotun Nappe, Southern Norway. In: Deformation Mechanisms in Nature and Experiment. Tectonophysics, 1999, 303: 223–249
20 Yan D P, Zhou M F, Song H L, et al. A geochronological constraint to the Guandi complex, Western Hills of Beijing, and its implications for the tectonic evolution (in Chinese). Earth Sci Front, 2005, 12: 332–337
21 Liu B, Ba J, Zhang L, et al. Zircon LA-ICP-MS U-Pb dating of metamorphism and anatexis of the Guandi Complex, Zhoukoudian Area, Beijing (in Chinese). Geol Sci Technol Info, 2008, 27: 37–42
22 Wang Y, Zhou L Y, Li J Y. Intracontinental superimposed tectonics—A case study in the Western Hills of Beijing, eastern China. Geol Soc Amer, 2011, 123: 1033–1055
23 Yan D P, Zhou M F, Song H L, et al. Mesozoic extensional structures of the Fangshan tectonic dome and their subsequent reworking during collisional accretion of the North China Block. J Geol Soc, 2006, 163: 127–142
24 Song H L. Characteristics of Fangshan metamorphic core complex, Beijing and a discussion about its origin (in Chinese). Geosci—J Chin Univ Geosci, 1996, 10: 149–158
25 Leake B E. Nomenclature of amphiboles: Report of the subcommittee on amphiboles of the International Mineralogical Association, Commission on New Minerals and Mineral Names. Can Mineral, 1997, 35: 219–247
26 Lin W W, Peng L J. The estimation of $Fe^{3+}$ and $Fe^{2+}$ contents in amphibole and biotite from EMPA data (in Chinese). J Changchun Univ Earth Sci, 1994, 24: 156–164
27 Holland T, Blundy J. Non-ideal interactions in calcic amphiboles and their bearing on amphibole-plagioclase thermometry. Contrib Mineral Petrol, 1994, 116: 433–447
28 Hammarstrom J M, Zen E. Aluminum in hornblende: An empirical igneous geobarometer. Am Mineral, 1986, 71: 1297–1313
29 Hollister L S, Grissom G C, Peters E K, et al. Confirmation of the empirical correlation of Al in hornblende with pressure of solidification of calc-alkaline plutons. Am Mineral, 1987, 72: 231–239
30 Johnson M C, Rutherford M J. Experimental calibration of the aluminum-in-hornblende geobarometer with application to Long Valley Caldera (California) volcanic rocks. Geology, 1989, 17: 837–841
31 Schmidt M W. Amphibole composition in tonalite as a function of pressure: An experimental calibration of the Al-in hornblende barometer. Contrib Mineral Petrol, 1992, 110: 304–310
32 Anderson L A, Smith D R. The effects of temperature and $f_{O_2}$ on the Al-in-hornblende barometer. Am Mineral, 1995, 80: 549–559
33 Tullis J. Deformation of feldspars. In: Ribbbe P H, ed. Reviews in Mineralogy—Feldspar Mineralogy. Mineral Soc Amer, 1983, 2: 297–323
34 Liu J L. Ductile deformation of marble. In: Zhou W Q, ed. International Symposium on Tectonic Evolution and Dynamics of Continental Lithosphere. The Third All-China Conference on Tectonics, 1987. 125
35 Yao L J, Yan D P, Hu L, et al. Structure style and temperature-pressure estimation of the detachment fault zone around Fangshan Dome, Western Hills of Beijing (in Chinese). Earth Sci—J Chin Univ Geosci, 2007, 32: 357–365
36 Ji M, Hu L, Liu J L, et al. Dynamic recrystallization and metamorphic conditions of main rock-forming minerals (in Chinese). Earth Sci Front, 2008, 15: 226–233